Potential Artifacts in Interpretation of Differential Breakthrough of Colloids and Dissolved Tracers in the Context of Transport in a Zero-Valent Iron Permeable Reactive Barrier

by Pengfei Zhang[1,5], William P. Johnson[1,4], Michael J. Piana[2], Christopher C. Fuller[2], and David L. Naftz[3]

Abstract

Many published studies have used visual comparison of the timing of peak breakthrough of colloids versus conservative dissolved tracers (hereafter referred to as dissolved tracers or tracers) in subsurface media to determine whether they are advected differently, and to elucidate the mechanisms of differential advection. This purely visual approach of determining differential advection may have artifacts, however, due to the attachment of colloids to subsurface media. The attachment of colloids to subsurface media may shift the colloidal peak breakthrough to earlier times, causing an apparent "faster" peak breakthrough of colloids relative to dissolve tracers even though the transport velocities for the colloids and the dissolved tracers may actually be equivalent. In this paper, a peak shift analysis was presented to illustrate the artifacts associated with the purely visual approach in determining differential advection, and to quantify the peak shift due to colloid attachment. This peak shift analysis was described within the context of microsphere and bromide transport within a zero-valent iron (ZVI) permeable reactive barrier (PRB) located in Fry Canyon, Utah. Application of the peak shift analysis to the field microsphere and bromide breakthrough data indicated that differential advection of the microspheres relative to the bromide occurred in the monitoring wells closest to the injection well in the PRB. It was hypothesized that the physical heterogeneity at the grain scale, presumably arising from differences in inter- versus intra-particle porosity, contributed to the differential advection of the microspheres versus the bromide in the PRB. The relative breakthrough (RB) of microspheres at different wells was inversely related to the ionic strength of ground water at these wells, in agreement with numerous studies showing that colloid attachment is directly related to solution ionic strength.

Introduction

Comparisons of breakthrough of colloids versus dissolved tracers in subsurface media are often made to determine whether they are advected differently in subsurface media (Buddemier and Hunt 1988; Champ and Schroeter 1988; Bales et al. 1989; Toran and Palumbo 1992; Harvey et al. 1993; McKay et al. 1993; Vilks and Bachinski 1996; Morley et al. 1998; Pang et al. 1998) and to elucidate the mechanisms of differential advection. Differential advection of colloids versus dissolved tracers may be explained by exclusion processes (de Marsily 1986; Wood et al. 1990; Rehmann et al. 1999). Dissolved tracers are sufficiently small to allow them to move into relatively small pore spaces in the subsurface media and enter many or all of the pores, depending on the size of the ion or molecule. Since colloids are much larger than dissolved tracers (e.g., μm versus nm), they may be restricted to the larger pores in the subsurface media. This exclusion from the small pore spaces may occur by virtue of the large size of colloids relative to sediment pore throats, or due to the relatively low diffusion constants of colloids. Since advection is greater in the larger pores, colloids are expected to travel faster on average than dissolved tracers in cases where zones of larger pore space occur together with a finer porous matrix. Differential advection may also derive from size or charge exclusion of the colloids from the slower velocities in the margins of pore spaces. In this paper the term differential advection refers to enhanced advection of colloids relative to dissolved tracers at any scale, e.g., pore scale or higher.

The comparison of breakthrough of colloids versus dissolved tracers is not straightforward mainly due to the different detection limits between colloids and dissolved tracers, and due to the interaction of colloids with sediment. Comparison of breakthrough of colloids versus dissolved tracers has been made in some cases without considering important differences in mechanisms governing their transport. In contrast to dissolved tracers, colloidal materials often undergo significant attenuation during transport, and mass recovered is often only a small fraction of the injected mass. Additionally, resolution of analysis is very different for colloids ver-

[1]University of Utah, Department of Geology and Geophysics, 135 South 1460 East, Salt Lake City, UT 84112

[2]U.S. Geological Survey, Water Resources Division, 345 Middlefield Rd., Menlo Park, CA 94025

[3]U.S. Geological Survey, Water Resources Division, 2329 West Orton Circle, West Valley City, UT 84119

[4]Corresponding author: (801) 581-5033; fax (801) 581-7065; wjohnson@mines.utah.edu

[5]Current address: New Mexico Institute of Mining and Technology, Department of Earth and Environmental Science, 801 Leroy Pl., Socorro, NM 87801

Received September 2000, accepted April 2001.

sus dissolved tracers. Although there may be exceptions, it is generally true that the detection limits for colloids are much lower than the detection limits for dissolved tracers. For example, common colloids such as bacteria, viruses, and microspheres can be analyzed to a few colloids per milliliter, and the relative concentration for colloids can span eight to nine orders of magnitude. In contrast, the relative concentration for dissolved tracers typically covers four to five orders of magnitude.

Studies that use the first arrival (first detection) of colloids versus dissolved tracers may incorrectly conclude faster colloid transport relative to the dissolved tracer due to the lower detection limit of colloids. To avoid artifacts from the detection limit, some studies have compared the timing of breakthrough of the highest concentration (peak) for dissolved tracers and colloids (Champ and Schroeter 1988; Harvey et al. 1993; Harvey et al. 1995; Vilks and Bachinski 1996; Morley et al. 1998; Pang et al. 1998). This approach may assume that the timing of the peak concentration represents the average travel time of the dissolved tracers and the colloids. This assumption holds for conservative dissolved tracers since they lack interaction with the subsurface media. However, this assumption may not hold for colloids, because interaction with the subsurface media can significantly reduce the mobile mass and in some cases can cause the breakthrough peak to shift to earlier times.

The effect of colloid interaction with subsurface media on timing of breakthrough is illustrated by simulation of the one-dimensional advection-dispersion reaction equation

$$\frac{\partial C}{\partial t} = D\frac{\partial^2 C}{\partial x^2} - v\frac{\partial C}{\partial x} - kC \qquad (1)$$

where C (ML^{-3}) is the aqueous colloid concentration, v (LT^{-1}) is the interstitial velocity of the particles, D (L^2T^{-1}) is the hydrodynamic dispersion coefficient, and k (T^{-1}) is a colloid deposition rate constant that represents irreversible attachment of colloids to the stationary phase. Colloid deposition in this case is simplified to follow irreversible first-order kinetics, a conceptualization appropriate to represent gross colloid behavior (Kretzschmar et al. 1997; Grolimund et al. 1998; Logan et al. 1999).

For a semi-infinite column free of colloidal particles at time zero with a unit pulse input, Equation 1 can be solved analytically (Grolimund et al. 1998):

$$C(x,t) = n_o e^{-kt}\frac{x}{2\sqrt{\pi t^3 D}}\, e^{\frac{(x-vt)^2}{4Dt}} \qquad (2)$$

where n_o ($ML^{-3}T$) is a normalization constant that represents the total mass of colloidal particles injected divided by the total volumetric flux (L^3T^{-1}). For a conservative dissolved tracer (k = 0) the first exponential function term becomes unity.

Simulated breakthrough curves (BTCs) for a colloid with a first-order deposition rate constant (e.g., $k = 6.0 \times 10^{-5}\ s^{-1}$, a deposition rate constant relevant to microsphere attachment to ZVI material in this study) and a conservative dissolved tracer (equivalent in all respects to the colloid except for a deposition rate constant equal to zero) in homogeneous media are presented in Figure 1. In Figure 1a it is seen that the depleted colloid mass that breaks through often requires the use of different concentration scales to compare colloid and dissolved tracer breakthrough. This figure shows that the colloid peak breaks through earlier than the tracer, indicating an apparent "faster" transport of the colloid relative to the

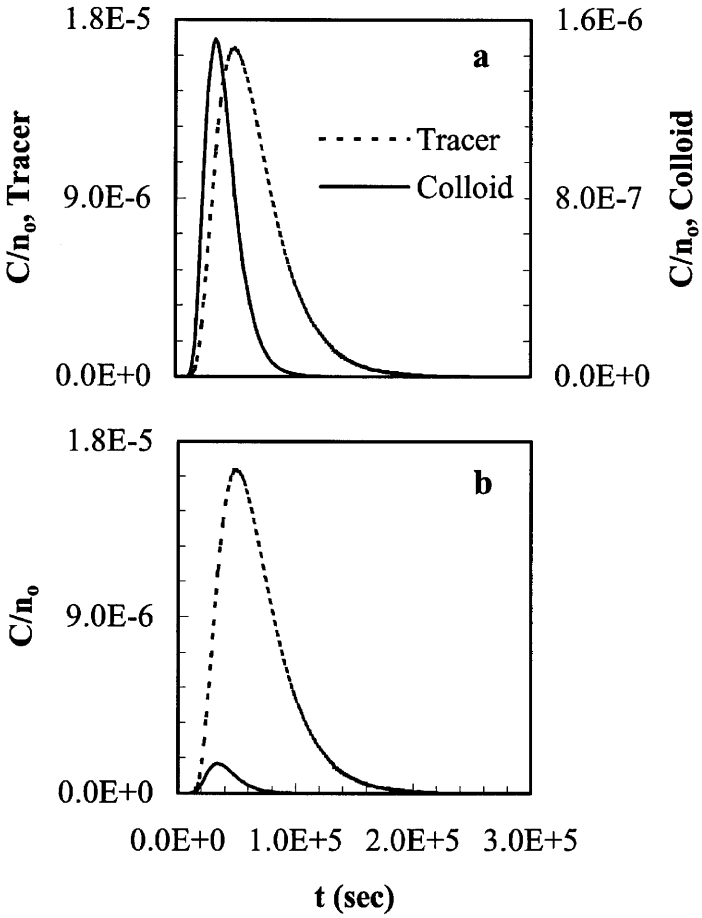

Figure 1. Computer simulated breakthrough curves for hypothetical dissolved tracer (k = 0) and colloid ($k = 6.0\times10^{-5}\ s^{-1}$) using Equation 2 with L = 0.4 m, $v = 6.0\times10^{-6}$ m/s, and $D = 2.5\times10^{-7}\ m^2$/sec; (a) different scales, (b) common scale. PV stands for pore volume.

dissolved tracer. Many comparisons of the timing of colloid and tracer breakthrough have used different colloid and tracer concentration scales (Champ and Schroeter 1988; Harvey et al. 1989; Harvey et al. 1995; Vilks and Bachinski 1996; Morley et al. 1998; Pang et al. 1998). In this format, however, the apparent earlier colloid breakthrough may be an artifact of "truncation" of colloid breakthrough due to colloid attachment. This artifact can be recognized by using a common scale to compare colloid and tracer concentrations (Figure 1b), where it is seen that significant colloid loss due to attachment shifts the colloid peak to earlier times despite no increase in the velocity of the colloid. This artifact was briefly mentioned in some studies (Harvey et al. 1995; Grolimund et al. 1998; DeBorde et al. 1999), but was not recognized in many other studies (Champ and Schroeter 1988; Vilks and Bachinski 1996; Morley et al. 1998).

The simplest way to determine differential advection of colloids relative to a dissolved tracer is to compare the normalized colloidal and tracer concentrations (C/C_o, where C_o is the influent colloid or tracer concentration) using a common scale. Normalized colloidal concentrations greater than the normalized tracer concentration between the first detection and peak arrival of tracer (i.e., anywhere on the rising limb of the tracer BTC) indicate differential advection of the colloid relative to the tracer. Becker et al. (1999) examined cumulative mass recovered for the same purpose. Comparison of normalized concentrations or mass recoveries for tracers and colloids is useful in cases where the colloid clearly exceeds the tracer. However, since colloid attachment lowers colloidal C/C_o (and

P. Zhang et al. GROUND WATER 39, no. 6: 2–xxx 2

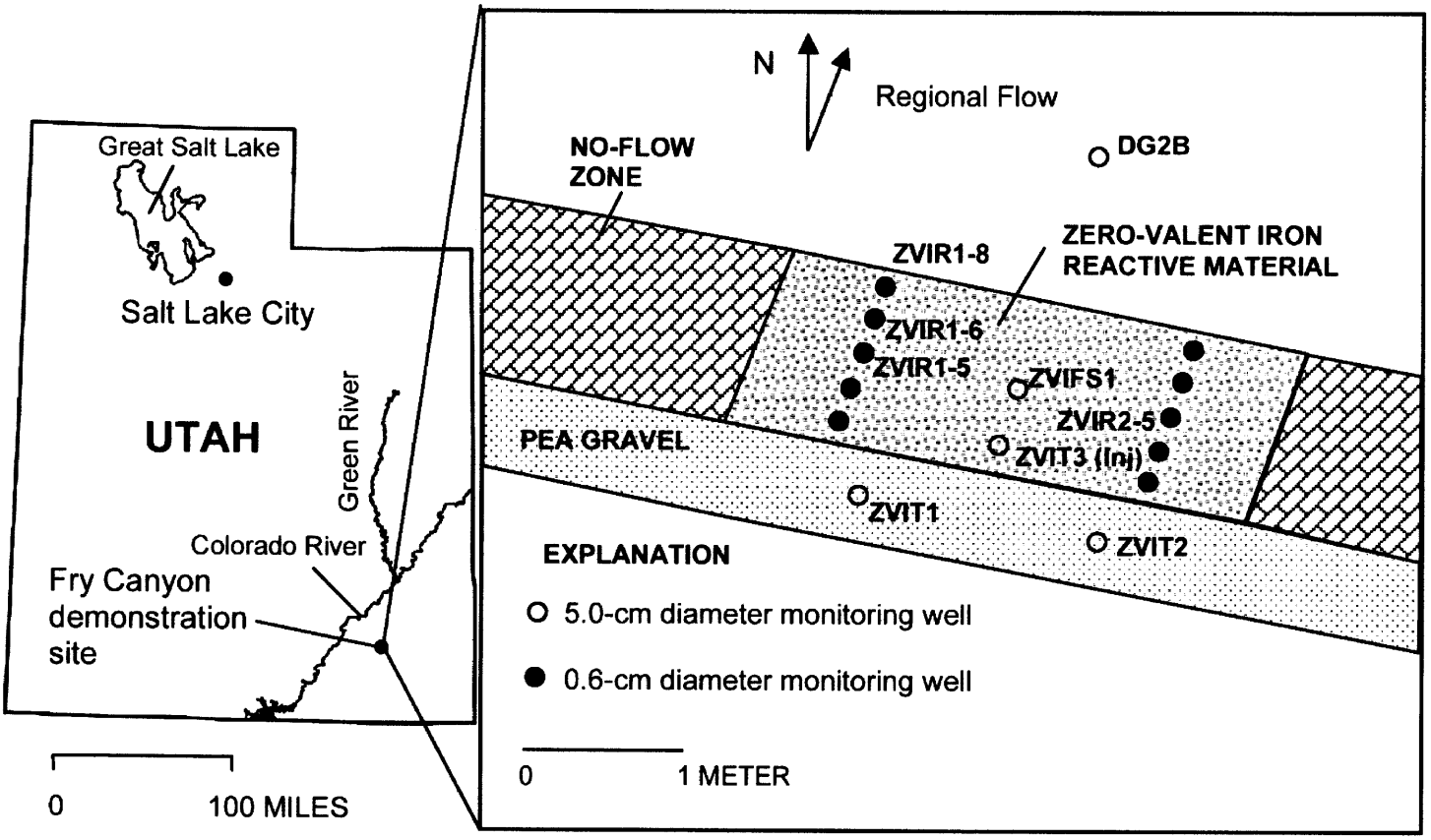

Figure 2. Schematic diagram of monitoring well placement within the ZVI barrier and location of the barrier within the state of Utah. The bromide and microspheres were injected into ZVIT3 and were monitored at ZVIFS1, ZVIR1-5, ZVIR2-5, ZVIR1-6, ZVIR1-8, and DG2B.

mass recovered), there may be cases where the colloid BTC lies below the tracer BTC but differential advection of the colloid may still have occurred. In other words, greater C/C_o (or mass recovery) for the colloid relative to the tracer after detection of the tracer is diagnostic, but it is not a necessary indicator of differential advection of the colloid.

In cases where colloid attenuation makes determination of differential advection more difficult, velocities representative of the colloid and the tracer may be derived by simulation (Equation 2) or moment analysis (first moment) of the BTCs to determine differential advection. However, many published analyses have not involved simulation or moment analysis of the BTCs, but have instead relied on visual qualitative comparison of the timing of peak breakthrough for colloids and tracers.

The purpose of this paper is to outline considerations in visual comparison of BTCs for colloids and dissolved tracers in order to avoid pitfalls arising from differences in their detection limits and their interaction with subsurface media. These considerations are implemented within the context of transport within a zero-valent iron-permeable reactive barrier located in Fry Canyon, Utah.

Simulation of the breakthrough data using the advection-dispersion-filtration equation (Equation 2) indicated that greater velocities were experienced by the microspheres relative to the bromide. A peak shift analysis that accounted for the effects of colloid attenuation on the timing of peak breakthrough was also implemented. The peak shift analysis yielded results that were equivalent to those of the analytical simulations. The peak shift analysis was applied in order to clarify considerations in performing visual comparison of the timing of peak breakthrough for the colloid and tracer.

Materials and Methods

Site Description

A zero-valent iron-permeable reactive barrier was installed in August 1997 to intercept uranium-contaminated ground water from an abandoned uranium upgrader operation near Fry Canyon, Utah (Figure 2). The shallow ground water in the colluvial aquifer contains elevated concentrations of uranium that exceed 20,000 µg/L (Naftz et al. 1999).

The colluvial aquifer, consisting of silt- to gravel-size particles, is up to 5.5 m thick, is saturated over the lower 1.5 m, and is situated over a bedrock confining layer. Pumping and slug tests on wells indicate that hydraulic conductivity values range from 1.52 to 15.2 m/day. Hydraulic-conductivity values measured in the laboratory on disturbed samples ranged from 16.8 to 25.9 m/day. The laboratory porosity of a repacked sample was 12.6%. Porosity values from the literature indicate the in situ effective porosity is probably 20% to 25% for mixed sand, gravel, and silt (Freethey et al. 1994).

The reactive material in the ZVI PRB consists of foamed aluminosilicate-bound pellets (~2 mm diameter) manufactured by Cercona of America. The hydraulic conductivity of this material prior to installation was 173.8 m/day and the total porosity (intra- + inter-particle porosity) was approximately 56% (Naftz et al. 2001), indicating significant internal porosity in the pellets. The effective porosity of the ZVI material was determined by gravimetric analysis.

A funnel-and-gate design was used to install the ZVI PRB. A trench intersecting the total saturated thickness of the colluvial aquifer was keyed into the underlying confining unit and backfilled with pelletized ZVI material. Impermeable walls on each side of the ZVI mate-

rial separated this PRB from two other PRBs concurrently installed on either side. The "as built" dimensions of the ZVI PRB are 2.13 m long by 0.91 m wide by 1.13 m deep (Figure 2). A 0.46 m wide layer of pea gravel was placed on the upgradient side of the ZVI PRB to facilitate uniform flow of contaminated ground water into the permeable gate structure. The ground water flux through the ZVI barrier was 0.82 m^3/day and the hydraulic gradient was approximately 0.003 (m/m). The hydraulic gradient is unlikely to have changed during the tracer test because of the high permeability of the ZVI barrier.

Sixteen 0.6 cm diameter schedule 40 PVC wells were installed along two parallel lines in the ZVI PRB parallel to regional flow (Figure 2). In addition, five 5 cm diameter schedule 40 PVC wells with 1.5 m screen intervals were placed in the pea gravel (ZVIT1 and ZVIT2), the ZVI PRB (ZVIT3 and ZVIFS1), and the colluvial aquifer (DG2B, Figure 2). Of these particular wells, one (ZVIT3) served as the injection well and six (ZVIFS1, ZVIR1-5, ZVIR2-5, ZVIR1-6, ZVIR1-8, and DG2B) served as the monitoring wells during this study. Of the 0.6 cm diameter monitoring wells, ZVIR1-5, ZVIR2-5, and ZVIR1-8 were screened over a 15 cm interval starting just above the bedrock, and ZVIR1-6 was screened over a 61 cm interval starting just above the bedrock. A sampling tube was permanently installed into each of the larger diameter (5 cm) wells and extended to about 15 cm from the bottom of the well screen. All screens were slotted pipe with slot size of 0.025 cm.

Transport Experiments

Fluorescent carboxylate modified latex paramagnetic microspheres (average diameter of 0.98 μm and density of 1.33 g/cm^3, Bangs Laboratories Inc.) and bromide (in the form of potassium bromide, KBr) were used as colloidal and dissolved tracers in this study. Ground water (47.3 L) was pumped from well ZVIT1 and was injected into ZVIT3 after addition of bromide (232 mg/L) and microspheres (1.0×10^7 spheres/mL). The tracer solution was injected by siphoning through a hose into a perforated pipe inserted into the injection well over the saturated interval. The injection volume was chosen to be equivalent to a cylindrical tracer plume (30 cm diameter) through entire saturated thickness of the PRB. Injection started at 10:30 a.m. MDT April 15, 1999, and was completed at 10:56 a.m. The transport experiment was conducted under natural gradient conditions.

Samples (200 mL each) were collected every three to four hours at a flow rate of 200 mL/min for bromide and microsphere analyses. Samples were collected manually using peristaltic pumps from all of the wells except ZVIR1-6 and ZVIR1-8. Samples from Wells ZVIR1-6 and ZVIR1-8 were collected via autosamplers installed in these wells. Each autosampler consisted of a peristaltic pump and a programmed timer that activated the pump. Each well had dedicated tubing for sample collection to avoid cross-contamination between wells. Well water was pumped through the peristaltic pump (200 mL for autosampler and 0.5 to 1 L for manual sampler) prior to sample collection to minimize cross-contamination of samples. All samples were stored in an icebox immediately after collection and refrigerated prior to analysis.

Bromide analyses were made by flow injection analysis at the U.S. Geological Survey. Microsphere concentration was analyzed ferrographically (Zhang and Johnson 1999; Zhang et al. 1999) at the University of Utah. The detection limit for bromide was 0.5 mg/L and the detection limit for microsphere was 2 spheres/mL. It should be noted that the microspheres become magnetic only in the presence of a strong external magnetic field.

Data Analysis

Simulation of the breakthrough data was performed using Equation 2. The values of v and D for the bromide were determined by least-squares fit to the field bromide data. The values of v, D, and k for the microspheres were determined by visual fit to the field microsphere data. Specifically, simulations with different values of v, D, and k were performed until the best match (determined visually) of the simulation and the field microsphere data was achieved. Travel distances were approximated by straight-line distances to the injection well, a reasonable approximation given the short travel distances and the relatively physically homogeneous barrier infill. The use of a one-dimensional expression to describe a three-dimensional site is justified by normalizing the microsphere flux to each well to the bromide flux. The microsphere n_o (Equation 2) was set equal to the bromide no to account for variability in ground water flux from well to well. In using a one-dimensional approach, the values of v, D and k represent average values across the flowpath.

Model efficiency E (Hornberger et al. 1992) was used as a measure of the goodness of fit of the model to the experimental data. The model efficiency is defined as

$$E = 1 - \frac{\sum(r_i)^2}{\sum(C_i - C_{av})^2} \quad (3)$$

where r_i is the ith residual between the predicted and the observed concentrations, C_i is the ith observed concentration, and C_{av} is the mean of the observed concentrations. A model efficiency of 1 indicates an ideal fit of the model to the observed data, while a model efficiency of 0 indicates a lack of fit.

For quantitative visual comparison of breakthrough data, the difference in timing of breakthrough of colloid versus dissolved tracer, Δt_{peak}, was defined as

$$\Delta t_{peak} = \frac{t_t - t_c}{t_t} \times 100 \quad (4)$$

where t_t and t_c are the times of arrival of peak concentrations of dissolved tracer and colloid, respectively.

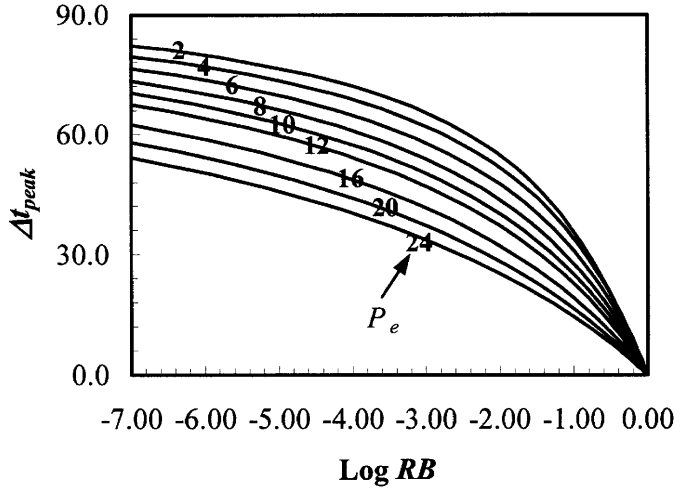

Figure 3. Δt_{peak} versus RB, with different lines for different values of P_e. The value of Δt_{peak} expected due to colloid attachment to the porous media (as accounted for by Equation 2) can be estimated using the appropriate curve (according to P_e) and the observed value of RB.

P. Zhang et al. GROUND WATER 39, no. 6: 4–xxx 4

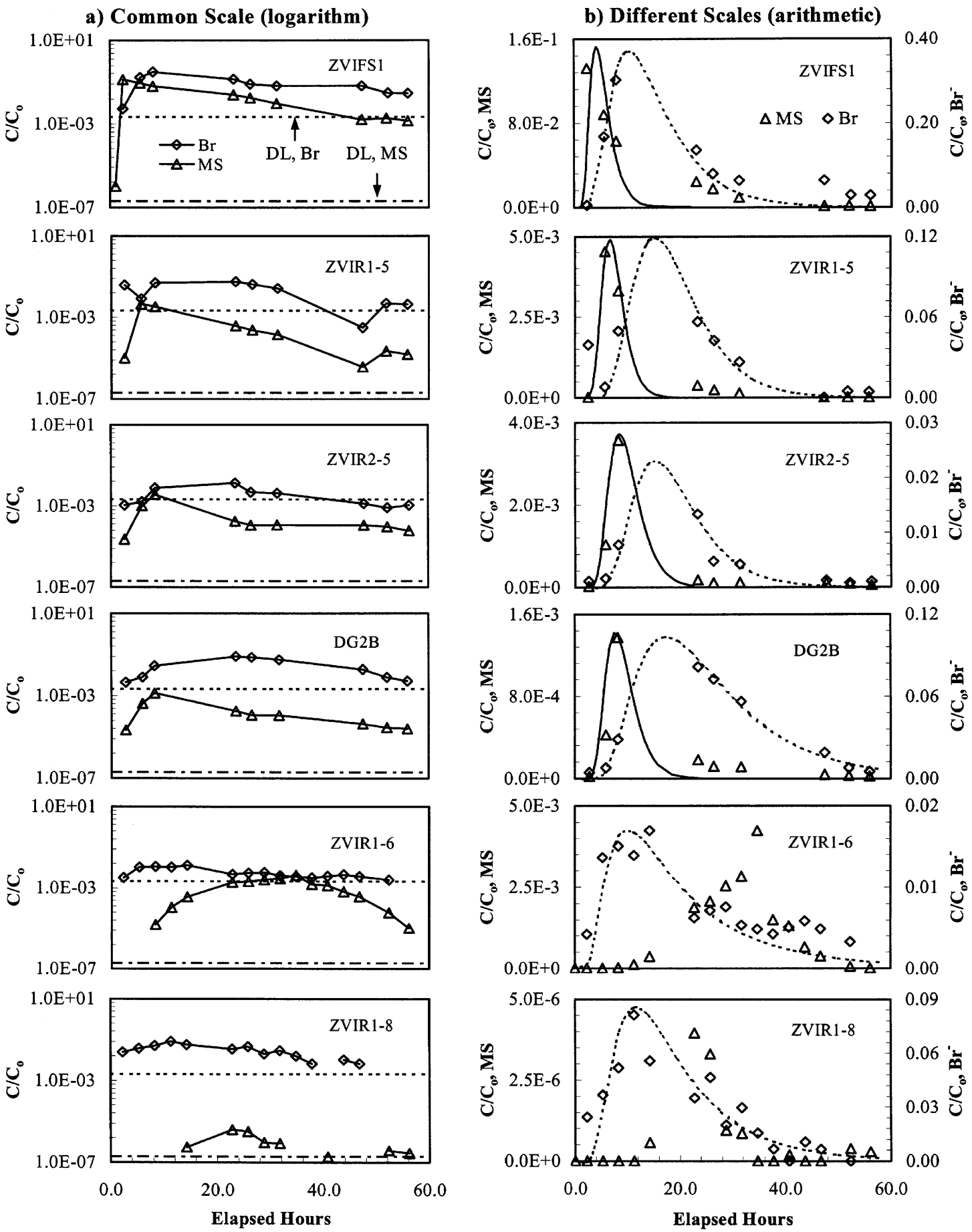

Figure 4. Microsphere (MS) and bromide (Br^-) breakthrough curves at various wells in and outside the ZVI barrier, (a) common scale, (b) different scales (left scale for MS and right scale for bromide). Detection limits (DL) for microspheres and bromide are shown as dashed lines. In part b bromide data were fit by least-squares method using Equation 2, while microsphere data were fit visually.

P. Zhang et al. GROUND WATER 39, no. 6: 5–xxx 5

Table 1
Transport Parameter Values Determined from Analysis of Field Data, and Results from the Peak Shift Analysis

Well ID	ZVIFS1	ZVIR1-5	ZVIR2-5	ZVIR1-6	ZVIR1-8	DG2B
Distance L (m)	0.304	0.549	0.549	0.646	0.761	1.810
v_{Br} (m/s)	5.5×10^{-6}	8.0×10^{-6}	8.0×10^{-6}	8.5×10^{-6}	1.1×10^{-5}	1.9×10^{-5}
v_{MS} (m/s)	1.0×10^{-5}	1.2×10^{-5}	1.1×10^{-5}	N/D	N/D	2.1×10^{-5}
D_{Br} (m^2/s)	2.2×10^{-7}	3.4×10^{-7}	3.3×10^{-7}	1.5×10^{-6}	1.5×10^{-6}	4.9×10^{-6}
D_{MS} (m^2/s)	4.0×10^{-7}	5.1×10^{-7}	4.6×10^{-7}	ND	ND	5.5×10^{-6}
k (s^{-1})	8.5×10^{-5}	1.3×10^{-4}	6.2×10^{-5}	ND	ND	1.0×10^{-4}
P_e	7.6	12.9	13.3	3.5	5.6	7.0
RB	0.13	0.014	0.075	0.21	0.000026	0.0038
Δt_{peak} observed	64	53	47	–191	–100	53
Δt_{peak} from Figure 3	24	33	24	ND	ND	50
Differential Advection?	Yes	Yes	Yes	No	No	No
Retardation?	No	No	No	Yes	Yes	No
E for Br	0.89	0.86	0.85	0.66	0.72	0.99
E for MS	0.58	0.98	0.94	ND	ND	0.73

ND stands for not determined.

In order to relate peak shift to attachment, the relative mass of colloid lost due to attachment must be known. The relative breakthrough, RB, of colloidal material versus dissolved tracer, observed at distance L is defined as (Harvey et al. 1989)

$$RB = \frac{\int_0^\infty \frac{C_{c(L,T)}}{C_{c,o}}\,dt}{\int_0^\infty \frac{C_t(L,t)}{C_{t,o}}\,dt} \quad (5)$$

where $C_c(L,t)$ and $C_t(L,t)$ are the concentrations of colloid and dissolved tracer at distance L and time t, respectively. $C_{c,o}$ and $C_{t,o}$ are the initial concentrations of colloid and dissolved tracers, respectively. The numerator and denominator in Equation 5 represent the areas under the colloid and tracer BTCs, respectively, when plotted as C/C_o versus time. The quantity RB thereby utilizes the flux of the tracer as a reference for the expected flux of colloidal material to a particular well. In the relatively homogeneous media of the PRB, the tracer can serve as a reasonable reference from which to determine the extent of attachment of the colloids en route to a given well.

The relationship between the magnitude of the peak shift (Δt_{peak}) and the value of RB depends upon the deposition rate constant (k), distance (L), average linear velocity (v), and hydrodynamic dispersion coefficient (D) as shown in Equation 2. As stated previously, the magnitude of the peak shift (Δt_{peak}) is directly related to RB, i.e., colloid attachment shifts the peak colloid breakthrough to earlier times (Figure 3). The values of L, v, and D can be combined into a Peclet number, P_e, where $P_e = vL/D$. For a given P_e number, the RB is inversely related to k, since the other variables that affect RB (v, L, and D) are held constant. Hence, for a given value of RB and P_e determined from experimental data, the peak shift expected from colloid attachment (as characterized by Equation 2) can be determined from Figure 3. In order to develop Figure 3, BTCs were simulated using Equation 2 for approximately 600 combinations of L, v, D, and k (L from 0.4 m to 2.0 m, v from 2.5×10^{-6} to 1.5×10^{-5} m/sec, D from 1.0×10^{-7} to 1.5×10^{-5} m^2/sec, and k from 5.0×10^{-6} to 6.4×10^{-4}/sec).

The strategy used to determine whether an observed Δt_{peak} represented differential advection was to estimate the Δt_{peak} expected from colloid attachment (using the same P_e as for the dissolved tracer), and then to compare this expected peak shift to the observed peak shift. If the observed peak shift was significantly greater than the peak shift expected from colloid attachment, then this indicated that the observed peak shift was not simply due to colloid attachment. The v (the P_e value) used in determining the peak shift expected from colloid attachment was the same as that for the tracer. Hence, it can be concluded that an observed peak shift greater than the peak shift expected from colloid attachment would be due to the colloid having a greater velocity than the tracer.

Results and Discussion

Differential Advection of Microspheres Relative to Bromide

The BTCs for microspheres and bromide transport in the PRB are shown using a common scale (a) and different scales (b) in Figure 4. Breakthrough simulations for bromide (dashed lines) and microspheres (solid lines) in Figure 4b represent the best fit of Equation 2 to the experimental data. The peak arrival time is subject to error due to insufficient experimental data and use of simulated curves. However, the simulated curves provide reasonable matches to the data, thereby providing a more accurate estimate of peak arrival relative to using the highest measured bromide or microsphere concentration. Equation 2 does not account for microsphere detachment and so cannot simulate extended microsphere tailing observed during elution.

When plotted under a common scale (Figure 4a), breakthrough at well ZVIFS1 showed higher normalized microsphere concentration relative to bromide concentration at t = 2.4 hours, indicating probable differential advection of microspheres. In contrast, the wells further downgradient (ZVIR1-5, ZVIR2-5, and DG2B) showed normalized microsphere concentrations that were always lower than the normalized bromide concentrations. Hence, for

P. Zhang et al. GROUND WATER 39, no. 6: 6–xxx 6

these wells it is not possible to determine whether differential advection of microspheres occurred simply by visual comparison of breakthrough.

When plotted using different scales for the microsphere and bromide BTCs (Figure 4b), peak microsphere concentrations clearly occurred at earlier times relative to bromide (Table 1) for wells ZVIFS1, ZVIR1-5, ZVIR2-5, and DG2B. However, it is necessary to account for the peak shift due to colloid attenuation in order to determine whether the observed peak shift represented differential advection of the microspheres. Simulation of breakthrough using Equation 2 accounted for potential effects of colloid attenuation on peak timing. The values of v determined from simulations of the breakthrough data (Table 1) indicated that during transport to wells ZVIFS1, ZVIR1-5, and ZVIR2-5 the microspheres experienced higher velocities relative to the bromide. At well DG2B the fitted velocities were similar for the microspheres and the bromide (i.e., there is no indication of differential advection in breakthrough data from this location).

In contrast to curve-fitting analyses, many analyses have relied upon qualitative visual comparison of the timing of peak breakthrough to determine whether differential advection is significant. Although qualitative visual comparison of the timing of peak breakthrough is pleasing in its simplicity, rigorous comparison requires accounting for the effect of colloid attenuation on the observed peak shift. To account for colloid attenuation in a visual format, the value of Δt_{peak} expected due to colloid attachment to the porous media (as accounted for by Equation 2) was estimated using the appropriate curve (according to P_e) and the observed value of RB (Figure 3). This value of Δt_{peak} expected due to colloid attachment was then compared to the Δt_{peak} observed from the experimental data (Table 1). The observed peak shift (Δt_{peak}) was much greater (> 20%) than the estimated Δt_{peak} for wells ZVIFS1, ZVIR1-5, and ZVIR2-5 (Table 1), indicating that the colloid experienced a greater velocity relative to the tracer. These data are in agreement with the relative velocities determined by simulations using Equation 2 (Table 1).

Model efficiency E values (Table 1) indicated that most of the simulations fit the experimental data very well (i.e., $E \geq 0.85$). The relatively low E values (~ 0.7) for bromide simulations for wells ZVIR1-6 and ZVIR1-8 were likely due to the outlier data in the elution limb of the BTCs, whereas the relatively low E values (0.6 to 0.7) for microsphere simulations for wells ZVIFS1 and DG2B were likely due to the inability of the model (Equation 2) to account for extended tailing of microsphere concentrations at those wells due to detachment of a subpopulation of the attached microspheres. Inability to account for mass recovered during extended tailing does not significantly affect our analysis, since the mass recovered during the extended tailing was small (at most 20%) relative to the mass recovered during breakthrough.

Errors associated with the peak shift analysis include (1) errors in RB estimation (integration of the areas under the breakthrough curves), (2) errors in D (and hence P_e) due to the assumption that D was equivalent for the colloid and tracer, and (3) errors in the observed Δt_{peak} (potential misrepresentation of the timing of the peak concentration due to limited data). However, the effects of the errors are limited. For example, the peak shift (Δt_{peak}) estimated from colloid attachment is not overly sensitive to RB (e.g., a 20% change in RB will cause about 5% change in Δt_{peak}, Figure 3), because Δt_{peak} is related to log RB. Likewise, although dispersion coefficients for colloids and dissolved tracers may differ, the difference is probably not large, i.e., less than a factor of two (Toran and Palumbo 1992; Grolimund et al. 1998; Morley et al. 1998). A factor of two underestimation of the dispersion coefficient translates to an underestimate of the P_e value by a factor of two. This underestimate causes an underestimate of about 10% in the estimated Δt_{peak} for the highest P_e values observed in this study (compare curves with $P_e = 12$ and $P_e = 24$ in Figure 3), and smaller errors for smaller P_e values. Errors associated with the observed Δt_{peak} vary depending on the sampling frequency. In this study it was recognized that an error of up to 15% could be associated with the observed Δt_{peak}. Hence, differences between the observed Δt_{peak} and the expected Δt_{peak} were considered significant only when the difference exceeded 20%.

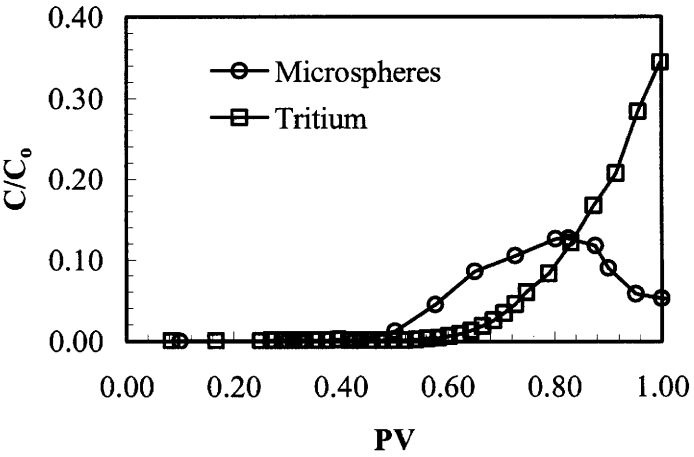

Figure 5. Microsphere and tritium breakthrough curves (up to 1 pore volume) for a laboratory column experiment with ZVI pellets. The normalized microsphere concentration was significantly higher than the normalized tritium concentration between 0.5 and 0.8 pore volume, indicating differential advection of microspheres.

The analytical and visual analyses were equivalent, differing only with respect to format of the analysis. Both analyses indicated that the observed peak shift in wells ZVIFS1, ZVIR1-5, and ZVIR2-5 may not have been solely due to colloid attachment (as accounted for in Equation 2), but instead may represent differential advection of the microspheres. In contrast to wells ZVIFS1, ZVIR1-5, and ZVIR2-5, well DG2B showed similar values for Δt_{peak} estimated from colloid attenuation and observed Δt_{peak} (Table 1), indicating that the observed earlier peak breakthrough of the microspheres relative to the bromide in this well may have been due to microsphere loss to the barrier and aquifer material.

The visual peak shift analysis was presented to relate quantitative and descriptive means of analysis for differential advection, and may have no greater utility than simulation by Equation 2. However, the analysis serves to highlight considerations in visual comparison of colloid and dissolved tracer breakthrough. The analysis may also be simpler to implement than curve fitting under conditions where the timing of colloidal peak breakthrough is well constrained by the experimental data.

The differential advection of the microspheres relative to bromide manifested in the data closest to the injection well may derive from the inability of the microspheres to sample all of the internal porosity of the ZVI pellets. This inability to move into the smaller pores may occur due to several attributes of the microspheres, including their relatively large size, their relatively low diffusion constants, and possible electrostatic repulsion with the ZVI pellets. That microspheres may be differentially advected through the ZVI material is also indicated by column experiments as shown in Figure 5.

P. Zhang et al. GROUND WATER 39, no. 6: 7–xxx 7

Figure 5 shows differential advection of the microspheres relative to tritium in the ZVI material during transport through a column (2.5 cm ID × 15 cm length) at 10 mL/hour.

Retardation of Microspheres Relative to Bromide

Peak concentration of microspheres appeared to be much later than the peak concentration of bromide for wells ZVIR1-6 and ZVIR1-8 (Figure 4), indicating retardation of microspheres occurred during transport to these wells. It is possible that the microsphere retardation was an artifact of the use of autosamplers (e.g., trapped gas), since microsphere retardation occurred only in the wells that had autosamplers. However, the autosampler consisted of a peristaltic pump and a programmed timer and worked equivalently to the manual sampler, which consisted of a peristaltic pump with no timer. Purge cycles were conducted in both the manual and automatic samplers. Hence, there is no obvious mechanism by which the autosamplers would cause apparent microsphere retardation at wells ZVIR1-6 and ZVIR1-8.

Retardation of colloids relative to dissolved tracers has been previously observed in several field studies (Harvey et al. 1995). Filtration and retardation are distinct breakthrough phenomena and may result from different mechanisms of attachment. The attachment mechanisms that result in filtration allow detectable colloid concentrations to pass through the system, and this may continue for extended periods of time. In contrast, the attachment mechanisms that result in retardation prevent passage of detectable colloid concentrations, but only for a relatively limited period of time. Attachment that results in retardation is limited in extent (becomes "shut off"), due either to reversibility of the attachment process (Harvey and Garabedian 1991) or due to limited numbers of attachment sites (Lindqvist et al. 1994; Johnson et al. 1995).

Effects of Colloid Attachment Mechanisms on Peak Shift

The analysis performed using Equation 2 to determine the expected value of Δt_{peak} due to filtration (first-order irreversible colloid attachment) is not applicable to situations where Δt_{peak} is negative (the colloid is retarded relative to the tracer). As shown in the analysis of Equation 2, filtration results in positive shifts in Δt_{peak} (Figure 1). In contrast, retardation results in negative shifts in Δt_{peak}. The peak shift analysis cannot separate the effects of these two phenomena on the breakthrough of colloids. For example, the similar estimated Δt_{peak} and observed Δt_{peak} for DG2B may result from various combinations of differential advection of colloids (positive shift in Δt_{peak}), filtration (positive shift in Δt_{peak}), and retardation (negative shift in Δt_{peak}). However, what the peak shift analysis does achieve is the recognition that observed earlier peak breakthrough of colloids relative to dissolved tracers may not indicate differential advection of the colloids. The analysis indicates that differential advection of microspheres relative to bromide tracer is indicated only in the data from wells ZVIFS1, ZVIR1-5, and ZVIR2-5, where the observed Δt_{peak} is much greater than the Δt_{peak} expected from filtration.

Generally, the difference between the observed peak shift and the peak shift expected from filtration decreased with distance from the injection well (Table 1). This indicates that any potential evidence of differential advection of colloids was increasingly obscured as travel distance increased. It can be speculated that the obscuring mechanism was retardation, by a mechanism that became significant only over larger transport distances in the system.

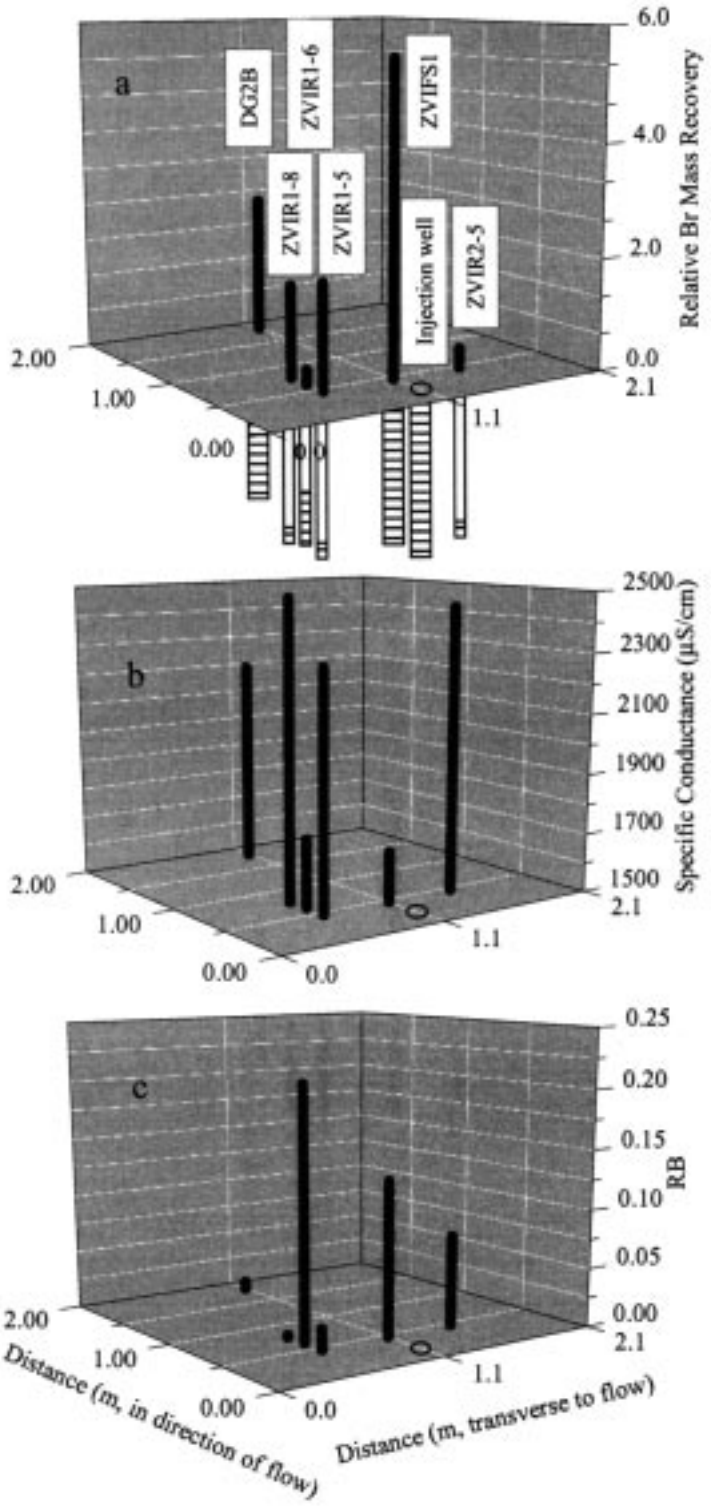

Figure 6. Three-dimensional plot of relative bromide recovery ($\int_0^\infty C_{Br}/C_{Br,o}dt$): (a), total iron (b), and RB, (c) for wells inside and outside the ZVI barrier. Well screen intervals are shown schematically. Wells ZVIR1-5, ZVIR2-5, and ZVIR1-8 have 15 cm screen intervals starting just above the bedrock, well ZVIR1-6 has a 61 cm screen interval starting from the bedrock, and wells ZVIFS1 and DG2B are screened over the entire barrier depth. Distances shown are parallel and transverse to regional flow.

Microsphere Breakthrough in Wells ZVIR1-6 and ZVIR1-8

The peak microsphere breakthrough in ZVIR1-8 apparently occurred earlier relative to ZVIR1-6 (compare in Figure 4b), despite the fact that ZVIR1-8 is located farther from the injection point. However,

P. Zhang et al. GROUND WATER 39, no. 6: 8–xxx 8

this did not necessarily indicate faster transport of microspheres to ZVIR1-8 than to ZVIR1-6, since the apparent earlier peak breakthrough in ZVIR1-8 may have been due to greater microsphere attachment en route to that well relative to ZVIR1-6. The greater microsphere attachment (due to filtration) en route to ZVIR1-8 was indicated by the much lower value of RB for that well (0.000026) relative to ZVIR1-6 (0.21). Since the microsphere attachment due to filtration shifts the peak breakthrough to earlier times (Figures 1 and 3), the greater microsphere attachment en route to ZVIR1-8 may have caused the apparent earlier microsphere breakthrough in that well relative to ZVIR1-6.

Bromide Mass Recovery and General Flow Direction

Wells ZVIFS1 and DG2B showed relatively high bromide mass recovery ($\int_0^\infty C_{Br}/C_{Br,o}dt$) (Figure 6a), indicating that these wells were located within the main flowpath through the barrier. However, only slightly lower mass recovery values in wells ZVIR1-5 and ZVIR1-8, and very low recovery in ZVIR2-5, indicate that the flow was not symmetric through the barrier, but was skewed to the north relative to the regional flow. The skewed flow direction was not likely an artifact of the increased pumping during sampling on the west side of the ZVI barrier, since the sample volumes were small and the sampling frequency was low. The low bromide mass recovery in ZVIR1-6 relative to the adjacent wells indicated low ground water flux to that location in the barrier.

Microsphere Relative Breakthrough (RB) and Ionic Strength

The differences in colloid RB among the various wells may be related to differences in ionic strength of ground water at these locations in the barrier. Figure 6b shows the specific conductance (indicative of ionic strength) at each well location. The values of specific conductance were not correlated to well screen length, indicating that the observed variations in specific conductance represented actual variations in geochemical conditions, rather than differing extents of ground water mixing due to variations in screen length. Figure 6c shows qualitatively that colloid RB is high (colloid attachment is low) in the wells where specific conductance (ionic strength) is low (Figure 6b), in agreement with numerous studies showing that colloid attachment is directly related to solution ionic strength (Fontes et al. 1991; Scholl and Harvey 1992; Ryan et al. 1999; Li and Logan 1999).

Conclusions

In summary, comparison of breakthrough of colloidal versus dissolved tracers must take into account interaction of the colloid with the porous media. Colloid attachment may shift the timing of peak colloid breakthrough toward earlier or later times depending on the mechanism of attachment. Expected peak shifts to earlier times due to colloid attachment can be estimated using Figure 3, and compared to observed peak shifts in order to determine whether the observed peak shifts can be at least partially attributed to differential advection. Our results in Fry Canyon indicated that physical heterogeneity at the grain scale, presumably arising from inability of the microspheres to enter the smaller pore spaces, contributed to the differential advection of microspheres relative to bromide in the PRB. However, this effect was manifested only in the BTCs from the monitoring wells situated closest to the injection well in the PRB.

Acknowledgments

Funding for this PRB installation was provided by the U.S. Environmental Protection Agency/Superfund and Office of Radiation and Indoor Air as part of a field demonstration of PRBs. The authors would like to thank T.D. Scheibe, M.W. Becker, L. Toran, W.R. Kelly, and an anonymous reviewer for critical reviews of an earlier version of this manuscript.

References

Bales, R.C., C.P. Gerba, G.H. Grondin, and S.L. Jensen. 1989. Bacteriophage transport in sandy soil and fractured tuff. *Appl. Environ. Microb.* 55, no. 8: 2061–2067.

Becker, M.W., P.W. Reimus, and P. Vilks. 1999. Transport and attenuation of carboxylate-modified latex microspheres in fractured rock laboratory and field tracer tests. *Ground Water* 37, no. 3: 387–395.

Buddemier, R.W., and J.R. Hunt. 1988. Transport of colloidal contaminants in groundwater: radionuclide migration at the Nevada test site. *Appl. Geochem*. 3, no. 5: 535–548.

Champ, D.R., and J. Shroeter. 1988. Bacterial transport in fractured rock —A field scale tracer test at the Chalk River nuclear laboratories. *Wat. Sci. Tech*. 20, nos. 11-12: 81–87.

DeBorde, D.C., W.W. Woessner, Q.T. Kiley, and P. Ball. 1999. Rapid transport of viruses in a floodplain aquifer. *Wat. Res*. 33, 2229–2238.

de Marsily, G. 1986. *Quantitative Hydrogeology: Groundwater Hydrology for Engineers*. San Diego: Academic Press.

Fontes, D.E., A.L. Mills, G.M. Hornberger, and J.S. Herman. 1991. Physical and chemical factors influencing transport of microorganisms through porous media. *Appl. Environ. Microbiol.* 57, 2473–2481.

Freethey, G.W., L.E. Spangler, and W.J. Monheiser. 1994. Determination of hydrologic properties needed to calculate average linear velocity and travel time of groundwater in the principal aquifer underlying the southeastern part of Salt Lake Valley, Utah. U.S. Geological Survey Water-Resources Investigations Report 92-4085.

Grolimund, D., M. Elimelech, M. Borkovec, K. Barmettler, R. Kretzschmar, and H. Sticher. 1998. Transport of in situ mobilized colloidal particles in packed soil columns. *Environ. Sci. Technol*. 32, no. 22: 3562–3569.

Harvey, R.W., L.H., George, R.L. Smith, and R.D. LeBlanc. 1989. Transport of microspheres and indigenous bacteria through a sandy aquifer: Results of natural and forced gradient tracer experiments. *Environ. Sci. Technol*. 23, 51–56.

Harvey, R.W., and S.P. Garabedian. 1991. Use of colloid filtration theory in modeling movement of bacteria through a contaminated sandy aquifer. *Environ. Sci. Technol*. 25, 178–185.

Harvey, R.W., N.E. Kinner, D. MacDonald, D.W. Metge, and A. Bunn. 1993. Role of physical heterogeneity in the interpretation of small-scale laboratory and field observations of bacteria, microbial-sized microsphere, and bromide transport through aquifer sediments. *Water Resour. Res*. 29, no. 8: 2713–2721.

Harvey, R.W., N.E. Kinner, A. Bunn, D. MacDonald, and D.W. Metge. 1995. Transport behavior of groundwater protozoa and protozoan-sized microspheres in sandy aquifer sediments. *Appl. Environ. Microb*. 61, no. 1: 209–217.

Hornberger, G.M., A.L. Mills, and J.S. Herman. 1992. Bacterial transport in porous media: Evaluation of a model using laboratory observations. *Wat. Resour. Res*. 28, 915–938.

Johnson, W.P., K.A. Blue, B.E. Logan, and R.G. Arnold. 1995. Modeling bacterial detachment during transport through porous media as a residence-time-dependent process. *Wat. Resour. Res*. 31, no. 11: 2649–2658.

Kretzschmar, R., K. Barmettler, D. Grolimund, Y. Yan, M. Borkovec, and H. Sticher. 1997. Experimental determination of colloid deposition rates and collision efficiencies in natural porous media. *Wat. Resour. Res*. 33, no. 5: 1129–1137.

Li, Q., and B.E. Logan. 1999. Enhancing bacterial transport for bioaugmentation of aquifers using low ionic strength solutions and surfactants. *Wat. Res.* 33, no. 4: 1090–1100.

Lindqvist, R., J.S. Cho, and C.G. Enfield. 1994. A kinetic model for cell density dependent bacterial transport in porous media. *Water Resour. Res*. 30, no. 12: 3291–3299.

Logan, B.E., T.A. Camesano, A.A. DeSantis, and K.M. Unice. 1999. Comment on "A method for calculating bacterial deposition coefficients using the fraction of bacteria recovered from laboratory columns." *Environ. Sci. Technol*. 33, 1316–1317.

P. Zhang et al. GROUND WATER 39, no. 6: 9–xxx 9

McKay, L.D., R.W. Gillham, and J.A. Cherry. 1993. Field experiments in a fractured clay till: 2. Solute and colloid transport. *Wat. Resour. Res*. 29, no. 12: 3879–3890.

Morley, L.M., G.M. Hornberger, A.L. Mills, and J.S. Herman. 1998. Effects of transverse mixing on transport of bacteria through heterogeneous porous media. *Wat. Resour. Res*. 34, no. 8: 1901–1908.

Naftz, D.L., J.A. Davis, C.C. Fuller, S.J. Morrison, G.W. Freethey, E.M. Feltcorn, R.G. Wilhelm, M.J. Piana, J.L. Joye, and R.C. Rowland. 1999. Field demonstration of permeable reactive barriers to control radionuclide and trace-element contamination in ground water from abandoned mine lands. In *U.S. Geological Survey Toxic Substances Hydrology Program—Proceedings of the Technical Meeting*, Charleston, South Carolina, March 8–12, 1999—Volume 1 of 3—*Contamination from Hardrock Mining*, ed. D.W. Morganwalp and H.T. Buxton, 281–288. *U.S.* Geological Survey Water-Resources Investigations Report 99-4018A.

Naftz, D.L., C.C. Fuller, J.A. Davis, S.J. Morrison, G.W. Freethey, E.M. Feltcorn, R.G. Wilhelm, M.J. Piana, R.C. Rowland, and J.E. Blue. 2001. Field demonstration of permeable reactive barriers to remove dissolved uranium from groundwater, Fry Canyon, Utah, September 1997 through September 1998. *U.S. Environmental Protection Agency Report*, in press.

Pang, L., M. Close, and M. Noonan. 1998. Rhodamine WT and *Bacillus subtilis* transport through an alluvial gravel aquifer. *Ground Water* 36, no. 1: 112–122.

Rehmann, L.L.C., C. Welty, and R.W. Harvey. 1999. Stochastic analysis of virus transport in aquifers. *Wat. Resour. Res*. 35, no. 7: 1987–2006.

Ryan, J.N., M. Elimelech, R.A. Ard, R.W. Harvey, and P.R. Johnson. 1999. Bacteriophage PRD1 and silica colloid transport in an iron oxide-coated sand aquifer. *Eviron. Sci. Technol*. 33, no. 1: 63–73.

Scholl, M.A., and R.W. Harvey. 1992. Laboratory investigations on the role of sediment surface and groundwater chemistry on the transport of bacteria through a contaminated sandy aquifer. *Environ. Sci. Technol*. 26, 1410–1417.

Toran, L., and A.V. Palumbo. 1992. Colloid transport through fractured and unfractured laboratory sand columns. *J. Contam. Hydrol*. 9, 289–303.

Vilks, P., and D.B. Bachinski. 1996. Colloid and suspended particle migration experiments in a granite fracture. *J. of Contam. Hyd.* 21, 269–279.

Wood, W., T. Kraemer, and P.P. Hearn Jr. 1990. Intragranular diffusion—An important mechanism influencing solute transport in clastic aquifers? *Science* 247, no. 4950: 1569–1572.

Zhang, P., and W.P. Johnson. 1999. Rapid selective ferrographic enumeration of bacteria. *J. of Magn. Magn. Mater*. 194, nos. 1–3: 267–274.

Zhang, P., W.P. Johnson, and R. Rowland. 1999. Bacterial tracking using ferrographic separation. *Environ. Sci. Technol*. 33, no. 14: 2456–2460.

P. Zhang et al. GROUND WATER 39, no. 6: 10–xxx 10